The following publication Y. Tan et al., "Hollow-Core Fiber-Based High Finesse Resonating Cavity for High Sensitivity Gas Detection," in Journal of Lightwave Technology, vol. 35, no. 14, pp. 2887-2893, 15 July15, 2017 is available at https://doi.org/10.1109/JLT.2017.2705229

Hollow-core fiber-based high finesse resonating cavity for high sensitivity gas detection

Yanzhen Tan, Wei Jin, *Senior Member*, *IEEE*, Fan Yang, Yun Qi, Congzhe Zhang, Yuechuan Lin, and Hoi Lut Ho

***Abstract*—High finesse hollow-core photonic bandgap fiber (HC-PBF) resonating Fabry-Perot gas cells are presented. These gas cells are made with a piece of HC-PBF sandwiched by two single mode fibers with mirrored ends. A HC-PBF cavity made with 6.75-cm-long HC-1550-06 fiber achieved a cavity finesse of 128, corresponding to an effective optical path length of ~5.5 m. Experiment with a 9.4-cm-long Fabry-Perot gas cell with a finesse of 68 demonstrated a detection limit of 7 p.p.m. acetylene. Compared with a single-path non-resonating HC-PBF, the use of a high finesse resonating HC-PBF cavity can reduce significantly the effect of modal interference on gas detection and improve the detection sensitivity. The cavity-enhanced HC-PBF gas cells enable stronger light-gas interaction and can be used to develop all-fiber gas sensors with high sensitivity and fast response.**

***Index Terms*—Gas sensor, photonic crystal fiber, Fabry-Perot resonator, optical fiber sensor.**

I. Introduction

Laser absorption spectroscopy (LAS) is a powerful technique for trace gas detection with high selectivity and sensitivity [1-4]. The employment of optical fiber-based technology enables reduction of apparatus size, remote interrogation and multiplexed multi-point detection [3-6].

The sensitivity of LAS sensors is proportional to absorption path length. Conventional optical fiber LAS gas sensors use micro-optic open-path absorption cells [5, 7, 8] and have difficulty in achieving long absorption path with compact size. Long path length may be achieved by using multi-pass White cells [9] and Herriott cells [10], they are however bulky, expensive and need lots of maintenance if used in the field. Cavity enhanced and cavity ring-down spectroscopies demonstrate very high sensitivity [11, 12], but they are also implemented with bulky free-space optical components and require complex alignment and mode matching optics.

A hollow-core photonic bandgap fiber (HC-PBF) has most of its optical power (>95%) propagating in the central hollow-core and allows strong light-gas interaction inside the fiber core [13, 14]. A HC-PBF can be coiled into small diameter with low-loss and used to construct long-path-length absorption cell with compact size. The use of HC-PBF for gas detection has been experimentally studied by a number of research groups [15-18] and achieved parts-per-million (p.p.m.) level detection sensitivity by using a 13-meter-long HC-PBF [19]. However, the response of the HC-PBF gas sensor is extremely slow due to the very long time needed for gas to fill the hollow-core [20]. Drilling side-holes along the length of HC-PBF helps to improve the response time [21-23], but it is difficult to achieve long-absorption-path (hence higher sensitivity) and fast response simultaneously because it would require an impractically large number of side-holes. Drilling of multiple side-holes by use of a femtosecond infrared laser has been demonstrated recently with an average loss of 0.02dB per hole. However, mode coupling was observed for increasing number of drilled holes, causing fluctuation in the transmitted light intensity that affects the signal to noise ratio (SNR) of sensors [24].

Here we present a novel HC-PBF-based high-finesse Fabry-Perot resonating absorption cell for high performance gas detection application. The Fabry-Perot absorption cell is made by jointing a piece of HC-PBF with two single mode fibers (SMFs) with mirrored ends, and light travels back and forth through the absorbing gas within the resonator and the effective absorption path length can be enhanced by a factor proportional to the cavity finesse. Such a resonating gas cell allows us to use a shorter HC-PBF (e.g., a few to tens of centimeters) to achieve high sensitivity, overcoming the problem of slow response associated with the use of long HC-PBF. The reduced cavity volume also minimizes the consumption of gas sample, which could be important for some applications. Moreover, the effect of mode interference noise in a resonating HC-PBF cavity is much smaller than in a single-path HC-PBF gas cell of the same length, which further improves the SNR of the gas detection system.

II. Basics of Cavity Enhancement

The basics of cavity enhancement with a high finesse Fabry-Perot resonating cavity as absorption cell may be explained with the aid of Fig. 1. We first consider an empty

Manuscript received March XXX, 2017; revised XXXX, 2017. This work was supported by the Hong Kong SAR government through GRF grant PolyU 152229/15E, Natural Science Foundation of China through NSFC grants 61535004 and 61290313, and the Hong Kong Polytechnic University through grants 4BCBE, 1ZVG4, and 4BCD1. Prof. Yi Jiang of Beijing Institute of Technology provides the SMF with coated mirrors in this work.

The authors are with the Department of Electrical Engineering, The Hong Kong Polytechnic University, Hung Hom, Kowloon, Hong Kong, and The Hong Kong Polytechnic University Shenzhen Research Institute, Nanshan District, Shenzhen, China. (e-mail: yanzhen.tan@connect.polyu.hk; wei.jin@polyu.edu.hk;ee.yangfan@connect.polyu.hk;yun.qi@connect.polyu.hk;congzhe.zhang@polyu.edu.hk;lin.yuechuan@connect.polyu.hk;eehlho@polyu.edu.hk).

Fabry-Perot cavity made by two identical mirrors separated by a distance of L, the transmission coefficient of the mirrors is denoted as t and the loss of the mirrors is l. The cavity finesse F may be expressed as [25, 26]

$$F = \frac{\pi}{t+l} \tag{1}$$

The resonant reflection R and transmission T of the cavity may be expressed respectively as [25]

$$R = \frac{P_r}{P_{in}} = (\frac{l}{t+l})^2 \tag{2}$$

$$T = \frac{P_t}{P_{in}} = (\frac{t}{t+l})^2 \tag{3}$$

where P_{in}, P_r and P_t represent input power, reflected power and transmitted power through the cavity, respectively.

A laser beam enters the gas absorption cell filled with a weakly absorbing gas, which travels back and forth (round-trip) many times inside the cell. Assuming that the gas absorption coefficient and concentration are respectively α and C, under the condition of $\alpha CL << t+l$, the resonant transmission as given in Eq. (3) may be re-written as

$$T' = \frac{P_t'}{P_{in}} \approx (\frac{t}{t+l})^2 (1 - \frac{2\alpha CL}{t+l}) \tag{4}$$

The absorption-induced relative change in the transmitted light signal through the cavity may be related to gas concentration by

$$S_{absorption} = \frac{P_t - P_t'}{P_t} = \frac{2\alpha CL}{t+l} = \frac{2F}{\pi} \cdot \alpha CL \tag{5}$$

Comparing this with a single-path non-resonating gas cell of the same length L, the use of a Fabry-Perot cavity with finesse F enhances the signal change by a factor of $2F/\pi$, giving an effective absorption path length of $(2F/\pi)L$. For example, if the cavity length L is 10 cm and finesse is 10^4, the effective absorption path length becomes 640 m, indicating that an extremely long effective path length and hence high detection sensitivity could be obtained by use of a high finesse cavity.

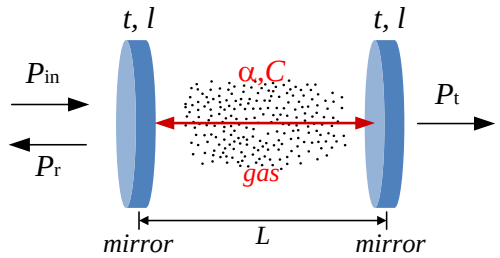

Fig. 1. Basics of cavity enhancement with a high finesse Fabry-Perot resonator for gas detection. P_{in}, P_r and P_t denote respectively the cavity input, reflected and transmitted light powers.

III. The HC-PBF Fabry-Perot Cavity

A schematic of the HC-PBF Fabry-Perot resonating gas cell is shown in Fig. 2(a). It is formed by sandwiching a length of HC-PBF between two mirrors made at the ends of two SMF pigtails. Fig. 2(b) shows the scanning electronic microscope (SEM) image of the HC-1550-06 fiber used in our investigation. It has a core diameter ~11 μm and was purchased from NKT Photonics. The SMF with coated mirrors are made by coating the ends of SMFs with alternating dielectric layers (SiO_2 and TiO_2) that have reflectivity of ~99%. The SMFs with mirrored ends are directly connected or spliced to the HC-PBF, without the need for mode-matching lenses. For the purpose of gas filling into the hollow-core, a small gap (<1 μm) can be kept at one or both of the HC-PBF/SMF joints. Alternatively, low-loss micro-channels may be made from the side of the HC-PBF to achieve faster gas filling into the hollow-core [23, 24].

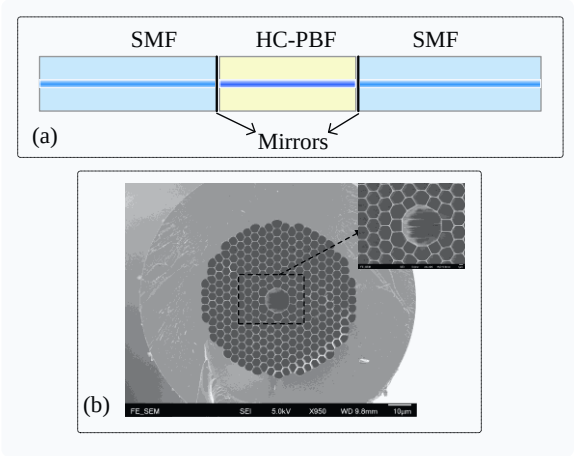

Fig. 2. (a) Schematic of a HC-PBF Fabry-Perot resonating gas cell. (b) Scanning electron microscopy (SEM) image of the HC-1550-06 fiber's cross-section.

The fabrication procedure of the HC-PBF Fabry-Perot gas cell is illustrated in Fig. 3: (a) a cleaved SMF fiber is inserted and fixed to a standard fiber ferrule with an inner diameter of 125 μm and an outer diameter of 2.5 mm, the assembly is then end-polished and coated with a dielectric mirror with reflectivity of ~99%. Similarly, a carefully cleaved HC-PBF is inserted into another ferrule and fixed to the ferrule with epoxy; (b) the two ferrules with fibers inserted are joint together by a mechanical splicer with an inner diameter of 2.5 mm, which aligns the two ferrules and holds them together tightly. A small gap (<1 μm) is left between the end-face of the HC-PBF and the mirrored end, and this small gap and the slit in the mechanical splicer facilitate gas filling into the HC-PBF. The ferrules and mechanical splicer are then fixed together with epoxy to form an integrated assembly; (c) the other end of the HC-PBF is similarly connected to a SMF with a mirrored end, and a Fabry-Perot gas cell is then constructed. We have made several such absorption cells with the length of HC-PBF ranging from 5 to 10 cm, but it is straightforward to make longer HC-PBF Fabry-Perot cells with this method.

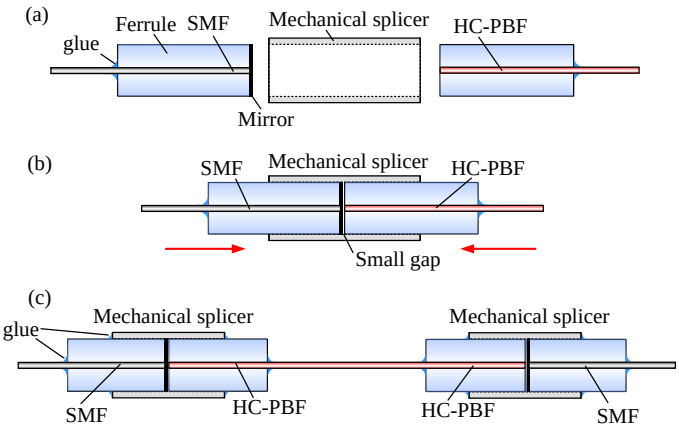

Fig. 3. Fabrication process of a HC-PBF Fabry-Perot gas cell.

The basic quantities characterizing a HC-PBF Fabry-Perot cavity are its free spectral range (*FSR*) which is the separation in frequencies (or wavelengths) between the two successive resonance modes, and the full-width half-maximum (FWHM) spectral width (δν) of the cavity resonances. The finesse of a cavity may then be determined by using [27]

$$F = \frac{FSR}{\delta\nu} \tag{6}$$

where $FSR=c/2nL$, n is the effective mode index of the HC-PBF and L the cavity length. For a hollow cavity length of 9.4 cm, the corresponding *FSR* is 12.5 pm at the wavelength of 1532 nm.

One method to characterize a HC-PBF Fabry-Perot cavity, including the measurement of its transmission spectrum and finesse, is to modulate the cavity length (or the laser wavelength) so that laser beam is periodically coupled into the cavity. Here we fix the laser wavelength and sweep the cavity length by a multilayer piezoelectric stack (PZT), allowing the laser wavelength to transmit through different cavity resonances one after the other in time. Fig. 4(a) shows the sweeping region in the cavity transmission (the yellow region) in which two adjacent cavity resonances are swept across a fixed laser wavelength (the red arrow) by sweeping the cavity length. Fig. 4(b) shows the experimental setup for characterizing the HC-PBF Fabry-Perot cavity. The HC-PBF section of the cavity is mounted on a multilayer PZT by nail enamel and two SMF pigtails of the cavity are connected to an external cavity diode laser (ECDL) and a photo-detector (PD), respectively. Fig.4(c) is the photo of the HC-PBF cavity with a PZT attached to it. The cavity length is swept by the PZT through applying a triangular voltage with magnitude of ~10.5 V and frequency of 1 Hz. Sweeping the cavity length allows the observation of the cavity transmission spectrum, which is recorded by a digital oscilloscope.

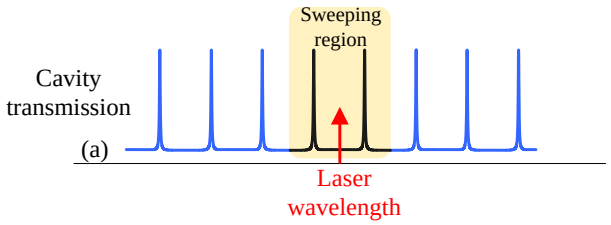

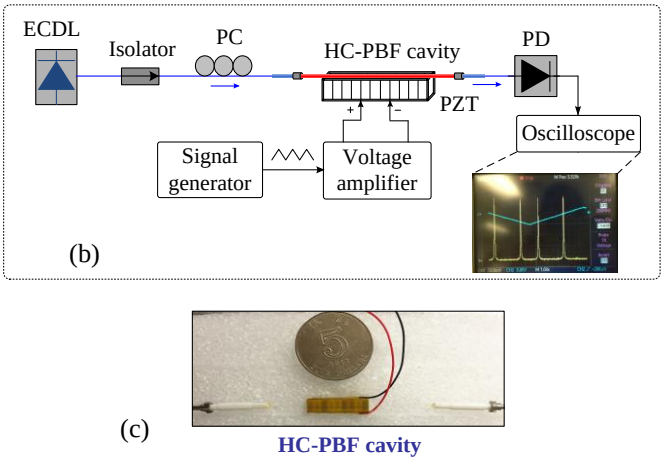

Fig. 4. (a) Schematic showing the sweeping region in the cavity transmission and a fixed laser wavelength. (b) Experimental setup for the characterization of a HC-PBF Fabry-Perot cavity. (c) A photo showing a HC-PBF Fabry-Perot cavity mounted on a multilayer PZT.

Figs. 5 (a) and (b) show the measured transmission spectrums of two HC-PBF Fabry-Perot gas cells with cavity length of 9.4 and 6.75 cm, respectively. In Fig. 5 (a), the laser wavelength is fixed to ~1532.8 nm, and the cavity finesse is calculated to be 68. This Fabry-Perot gas cell could in principle enhance the optical path length by a factor of $2x68/\pi$, giving an effective path length of 4.1 m. Similarly, in Fig. 5 (b), the laser wavelength is fixed to ~1530.3 nm, and the finesse is calculated to be 128, corresponding to an effective optical path length of 5.5 m.

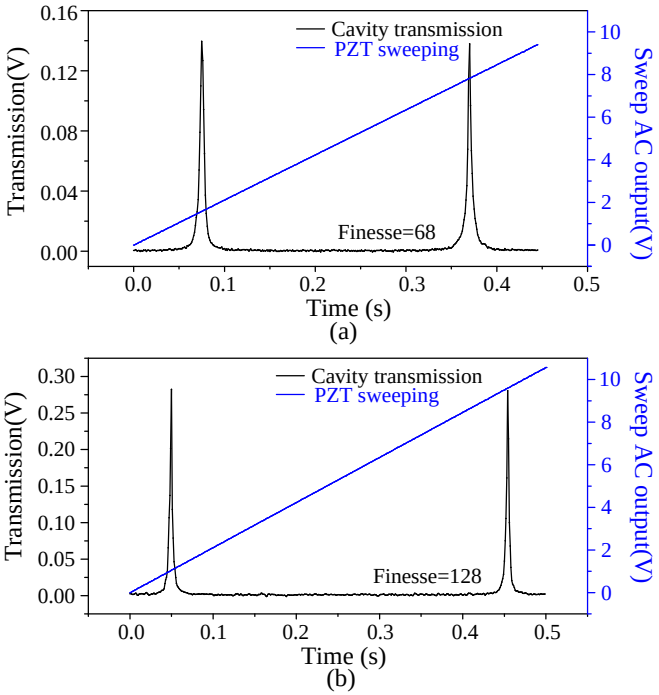

Fig. 5. Measured transmission spectrums of HC-PBF Fabry-Perot gas cells with cavity length of (a) 9.4 cm and (b) 6.75 cm.

It should be mentioned that the transmission spectrums are polarization dependent and can be adjusted by the polarization controller (PC) shown in Fig. 4(a). This may be because the HC-PBF has residual birefringence as has been observed

previously [28, 29]. Take the 9.4-cm-long HC-PBF Fabry-Perot cavity as an example, the transmission spectrums measured by repeatedly sweeping the cavity length when the PC is adjusted is shown in Fig. 6(a). Two resonances were observed within one FSR. The resonance peak denoted as "Peak 1" is strongest when the other resonance "Peak 2" disappears, and vice versa. For a clearer observation, the peak values of the two resonances in Fig. 6(a) are plotted in Fig. 6(b) as red squares and black dots, respectively. The two sets of resonant peaks represent two polarization eigenstates of the HC-PBF and are orthogonal to each other. Fig. 6(c) shows the transmission spectrums of the Fabry-Perot resonator when the orientation of the incident light is parallel to one of the polarization eigenstates of the HC-PBF. The magnitude of Peak 1 is ~3.5 times higher than that of Peak 2, indicating the two eigenstates have different losses. The measured finesses for the two polarization states are 68 and 38, respectively. From Fig. 6(c), the phase difference $\Delta\delta$ between the two polarization eigenstates is estimated to be $2\pi\times(51/297)=1.079rad$ at λ~1532.8 nm. Hence the residual birefringence of the HC-PBF (Δn) may be calculated to be [30]

$$\Delta n=\frac{\lambda\cdot\Delta\delta}{4\pi L}=1.4\times10^{-6} \quad (7)$$

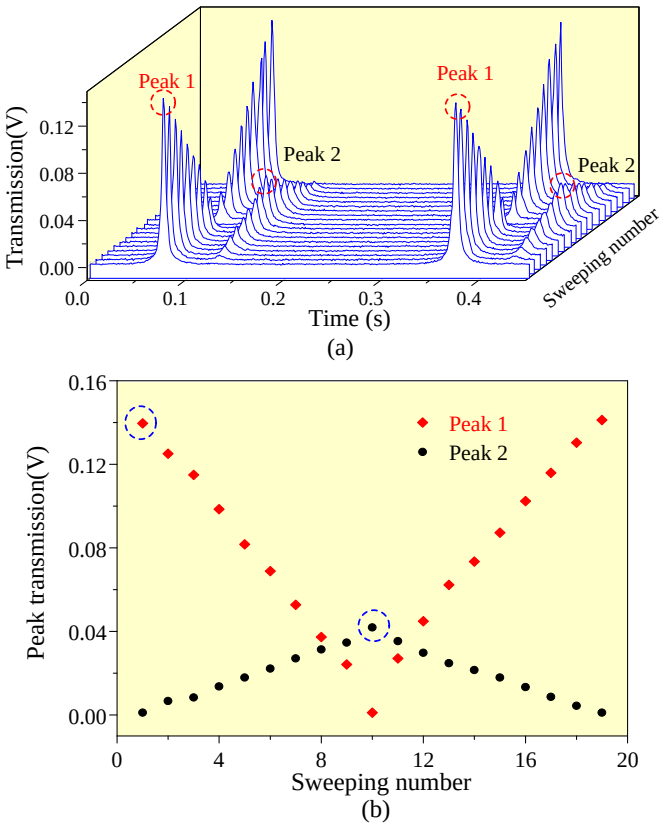

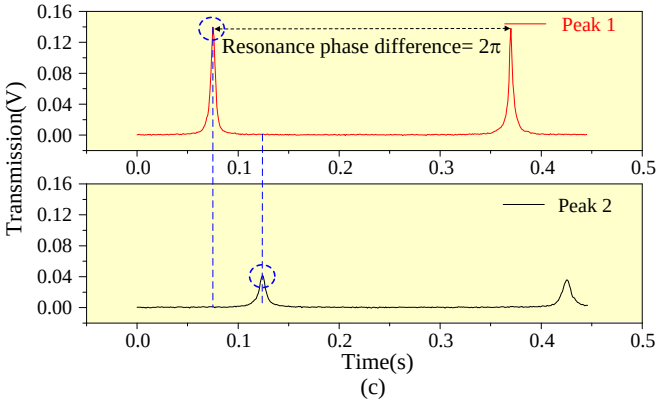

Fig. 6. (a) Measured evolutions of transmission spectrums of a HC-PBF resonating cavity when the input polarization is tuned continuously. (b) Peak values for Peaks 1 and 2 in (a). (c) Measured transmission spectrums when the polarization is parallel to one of the eigenstates.

IV. Gas Detection with HC-PBF Fabry-Perot Cavity

Gas detection experiments were conducted with the experimental setup shown in Fig. 7. The gas cell used is 9.4-cm-long with FSR of 12.5 pm (1.6 GHz) and finesse of 68. The absorption line used is the P(13) line of acetylene at 1532.83 nm, and the linewidth of this line is 41.26 pm (5.28 GHz) which covers approximately 3.3 FSR of the HC-PBF Fabry-Perot cavity, as indicated in Fig. 8(a). A distributed feedback (DFB) semiconductor laser is used as the light source and its nominal wavelength can be changed by thermal tuning and simultaneously modulated at a higher frequency via injection current modulation.

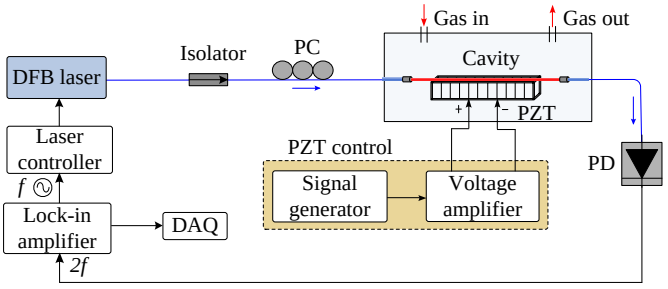

Fig. 7. Experimental setup for gas detection with a HC-PBF Fabry-Perot resonating gas cell. Blue line, optical fiber; black line, electrical cable; DFB, distributed feedback laser; PC, polarization controller; PZT, piezoelectric stack; PD, photo-detector; DAQ, data acquisition.

Before gas detection experiments, we apply a DC voltage to the PZT stack to tune the cavity length of the HC-PBF Fabry-Perot resonator, so that one of the cavity resonances is aligned to the center of the gas absorption line. The procedure is as follows: the wavelength of the DFB laser is firstly tuned to around the P(13) line and the wavelength is then scanned or swept to observe the cavity resonances around the absorption line. The cavity resonances are typically not aligned to the absorption line (as shown Fig.8a) but with a proper voltage (~3.5 V in our experiment) applied to the PZT, one of the resonances can be made to align to the center of the line at 1532.83 nm, indicated as Resonant A in Fig. 8(b). This cavity resonance is used for the gas detection experiment, which will be described later in this section. The DFB laser can be also tuned to another cavity resonance (Resonance B, around

1532.95 nm) away from the gas absorption, and the experiments are repeated at this resonance and compared with the results obtained at 1532.83 nm.

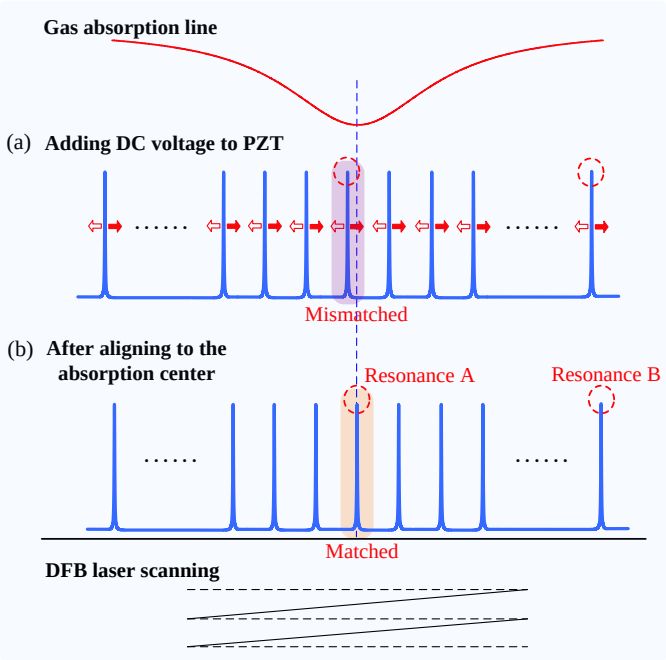

Fig. 8. Schematics showing the process of aligning a cavity resonance to the center of a gas absorption line. (a) Cavity resonances are not aligned to the absorption line, (b) one of the resonances (Resonance A) is aligned to the center of an absorption line. Resonance B is an arbitrary resonance with minimum absorption. The wavelength of the DFB laser is scanned to observe the resonances.

Filling gas sample into the HC-PBF Fabry-Perot resonating cell would shift the cavity resonance slightly due to variation in gas composition as well as temperature. The voltage applied to the PZT would then need to be fine-tuned to match the cavity resonance to the center of the absorption line. We then conducted acetylene detection experiment with wavelength modulation spectroscopy and lock-in detection. The DFB laser wavelength was scanned across the Fabry-Perot cavity resonance at the center of the P(13) absorption line (Resonance A) and at the same time, it was modulated sinusoidally at frequency of 22.1 kHz with amplitude of 4 mV. During the scanning, the second-harmonic of the modulation signal (i.e., at 44.2 kHz) was detected by use of the lock-in amplifier. The laser power into the absorption cell was ~1.63 mW and acetylene concentration was ~550 p.p.m.. The time constant of the lock-in amplifier is set to 300 ms with a filter slope of 18 dB/Oct. All the experiments were carried out at atmospheric pressure and room temperature. The experiment was repeated for Resonance B, which is away from the gas absorption line.

Figs. 9 (a) and (b) show the second harmonic lock-in outputs when the laser wavelength was scanned across Resonance A and Resonance B, respectively. The black lines are for the cavity filled with air while the red lines are for the cavity filled with 550 p.p.m. acetylene balanced by nitrogen. At Resonance A shown in Fig. 9 (a), the signal variation due to absorption by acetylene is 1.47 mV, corresponding to an absorbance of 1.47 mV/6.84 mV=21.5%. At Resonance B in Fig. 9 (b), the signal variation is negligible.

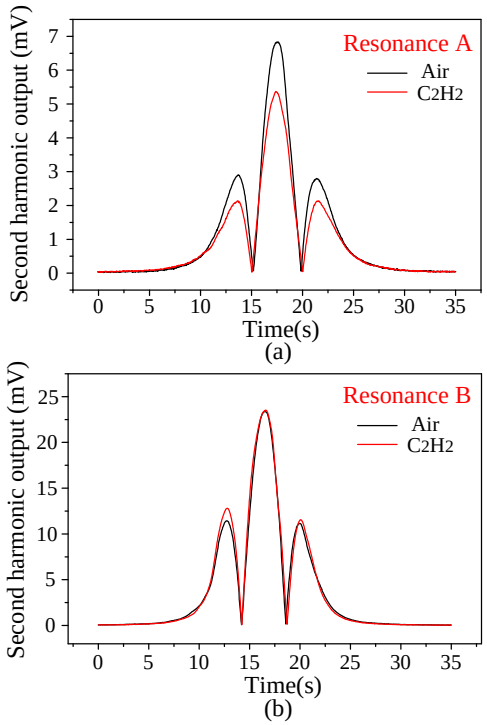

Fig. 9. Experimental results. (a) Second harmonic lock-in output signals when laser is tuned across a Fabry-Perot resonance at the center of the P(13) line of acetylene at 1,532.83 nm (Resonance A). (b) Second harmonic lock-in output signals when laser is tuned across a Fabry-Perot resonance away from the center of the P(13) line of acetylene at 1,532.95 nm (Resonance B). The black and red curves are respectively for the cavity filled with air and 550 p.p.m. acetylene balanced by nitrogen.

Experiments were repeated for different gas concentration of 357 and 725 p.p.m., and the absorption signal (%) as function of gas concentration is plotted in Fig. 10. Curve fitting shows that it has a linear relationship (r^2=0.9846) with a slope coefficient of 0.039% per p.p.m.. Based on HITRAN 2004 database, the equivalent absorption length of the cavity is determined to be ~378 cm [31], corresponding to an enhancement factor of $2F/\pi$ = 40 or a finesse of F = 62. This value is in agreement with the directly measured value of 68 in Section III.

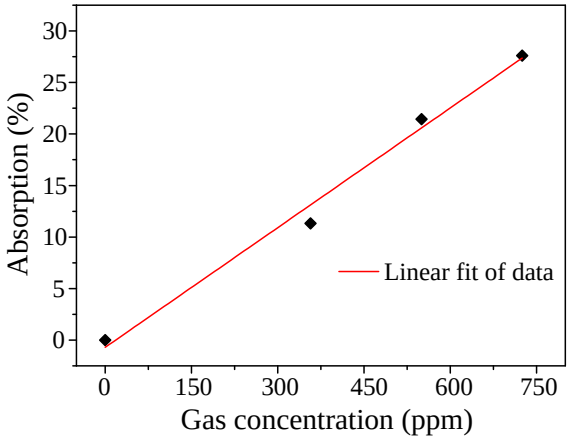

Fig. 10. Absorption signal (%) as function of gas concentration. Black squares: Experimental data. Red line: Linear fitting.

We also evaluated the fluctuation of second harmonic peak signal by repeatedly sweeping the resonance at 1532.83 nm over a period of 8 min when the gas cell is filled with air. The results are shown in Fig. 11. The standard deviation (s.d.) of fluctuation is 18.8 μV, giving a signal to noise ratio (SNR) of 1.47 mV/0.0188mV=78 when the cavity is filled with 550 p.p.m. acetylene. This corresponds to an error in the gas concentration measurement of 7 p.p.m. for a SNR of unity, or an equivalent absorption-coefficient (NEA) of $7.35\times10^{-6}cm^{-1}$.

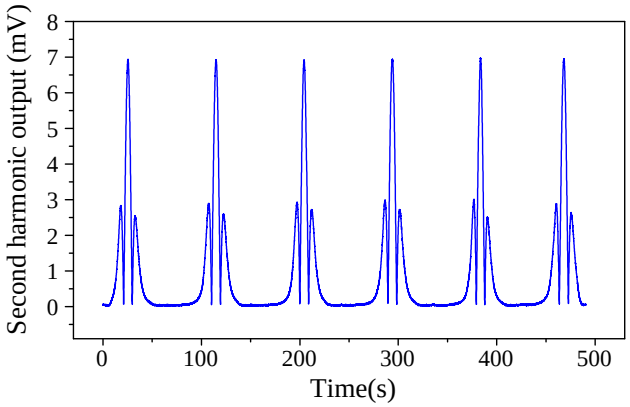

Fig. 11. Second harmonic lock-in output when the DFB laser wavelength is repeatedly scanned across the resonance at 1532.83 nm for ~500 s duration. The time constant of the lock-in amplifier is 1s with a filter slope of 18dB Oct^{-1}.

V. Comparison with a Single-Path HC-PBF Cell

To compare the performance of the resonating HC-PBF cavity with a non-resonating HC-PBF cell, we also conducted the experiment with a 10.8-cm-long HC-PBF (single-path, without mirrors). The cell was prepared by fusion splicing one end of the HC-PBF to a standard SMF while the other end butt-coupled to another SMF by use of an Ericsson FSU-975 fusion splicer. The transmission spectrum of the cell was measured with the experimental setup shown in Fig. 12(a). The external cavity diode laser (ECDL) and photo-detector (PD) are parts of an Agilent 81910A Photonic All-Parameter Analyzer. The wavelength of the ECDL was tuned from 1525 to 1535 nm with a resolution of 1 pm.

The measured transmission spectrum of the single-path HC-PBF cell and its Fourier transform are shown respectively in Figs. 12(b) and (c). The quasi-periodic spectrum is due to interference between the fundamental core mode and different groups of higher order modes, which are labeled in the inset of Fig. 12(c). Such modal interference was found to be a main factor that limits the performance of HC-PBF based sensors since current commercial HC-PBFs support several groups of modes and the interference of these modes results in intensity fluctuation of the transmitted light [6, 19, 32, 33]. The use of a longer HC-PBF (e.g., >10 m) would reduce the MI considerably but for the short sample investigated here the intensity fluctuation is large, causing large error in gas concentration measurement. A previous experiment with a 7-cm long HC-PCF single-path gas cell demonstrated a NEC of 647 p.p.m. methane [23], or $1.63\times10^{-4}cm^{-1}$ in NEA, which is significantly worse than the results we obtained here with the high finesse HC-PBF Fabry-Perot cavity gas cell. For the Fabry-Perot cavities reported here, the effect of MI on gas detection is found being reduced significantly since the higher order modes suffer much larger loss after traveling many times within the high finesse cavity.

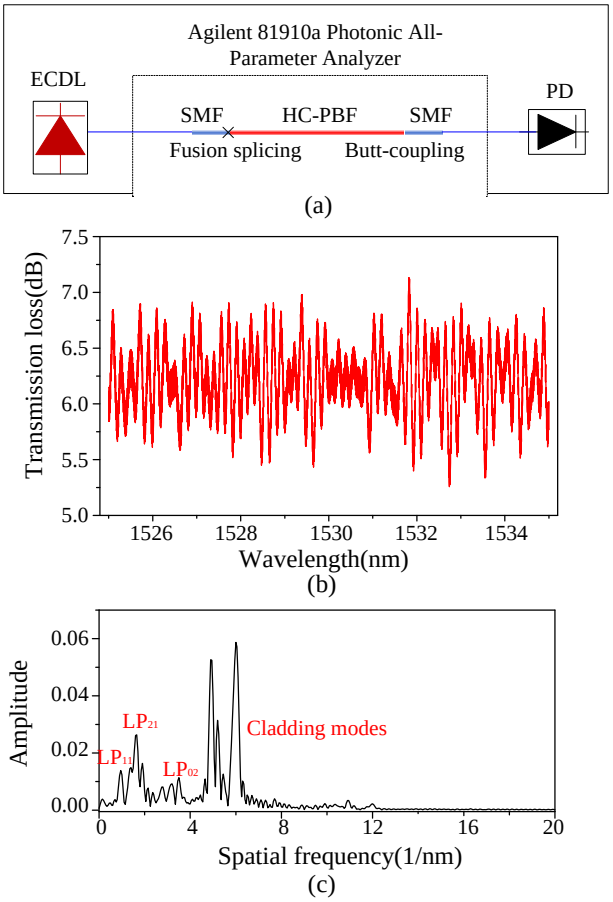

Fig. 12. (a) Experimental setup for measuring the transmission spectrum of a single-path HC-PBF cell. (b) Measured transmission spectrum of the HC-PBF cell. (c) Fourier transform of the spectrum in (b).

VI. Conclusion

In summary, we have presented all-fiber resonating gas cells based on HC-PBFs spliced to pigtail SMFs with mirrored ends. The high reflectivity mirrors (~99%) form high finesse Fabry-Perot cavities, which achieves long effective path length with relatively short HC-PBF gas cells. The enhancement factor is proportional to the cavity finesse. We have made several HC-PBF Fabry-Perot gas cells with length from 5 to 10 cm and cavity finesses from 50 to well over 100, achieving effective path length of several meters. Such gas cells achieve long effective path length with short length of HC-PBFs, enabling gas sensors with high sensitivity and fast response.

Comparing with the single-path (without mirrors) HC-PBF gas cells of a similar length, the high finesse HC-PBF Fabry-Perot cavity reduces significantly the effect of modal interference noise on gas detection. With a cavity length of 9.4 cm and finesse of 68, we demonstrated acetylene detection with a detection limit of ~7 p.p.m, 1-2 orders of magnitude better than a single-path HC-PBF sensor with a similar length [23] and comparable with that of a 13-m-long HC-PBF sensor [19]. With a true single mode HC-PBF and by locking the cavity

resonance precisely to the center of a gas absorption line, further improvement in performance is possible.

REFERENCES

[1] P. Werle, F. Slemr, K. Maurer, R. Kormann, R. Mücke, and B. Jänker, "Near-and mid-infrared laser-optical sensors for gas analysis," *Opt. Laser. Eng.*, vol. 37, pp. 101-114, 2002.

[2] U. Willer, M. Saraji, A. Khorsandi, P. Geiser, and W. Schade, "Near-and mid-infrared laser monitoring of industrial processes, environment and security applications," *Opt. Laser. Eng.*, vol. 44, pp. 699-710, 2006.

[3] J. Shemshad, S. M. Aminossadati, and M. S. Kizil, "A review of developments in near infrared methane detection based on tunable diode laser," *Sen. Actuators B*, vol. 171, pp. 77-92, 2012.

[4] J. Hodgkinson and R. P. Tatam, "Optical gas sensing: a review," *Meas. Sci. Technol.*, vol. 24, p. 012004, 2013.

[5] B. Culshaw, G. Stewart, F. Dong, C. Tandy, and D. Moodie, "Fibre optic techniques for remote spectroscopic methane detection—from concept to system realisation," *Sen. Actuators, B*, vol. 51, pp. 25-37, 1998.

[6] W. Jin, H. Ho, Y. Cao, J. Ju, and L. Qi, "Gas detection with micro-and nano-engineered optical fibers," *Opt. Fiber Technol.*, vol. 19, pp. 741-759, 2013.

[7] K. Chan, H. Ito, H. Inaba, and T. Furuya, "10 km-long fibre-optic remote sensing of CH4 gas by near infrared absorption," *Appl. Phys. B*, vol. 38, pp. 11-15, 1985.

[8] J. Dakin, C. Wade, D. Pinchbeck, and J. Wykes, "A novel optical fibre methane sensor," Proc. SPIE 0734 in *Fibre Optics' 87*, 1987, pp. 254-260.

[9] J. U. White, "Very long optical paths in air," *JOSA*, vol. 66, pp. 411-416, 1976.

[10] D. R. Herriott and H. J. Schulte, "Folded optical delay lines," *Appl. Opt.*, vol. 4, pp. 883-889, 1965.

[11] A. O'Keefe and D. A. Deacon, "Cavity ring-down optical spectrometer for absorption measurements using pulsed laser sources," *Rev. Sci. Instrum.*, vol. 59, pp. 2544-2551, 1988.

[12] T. McGarvey, A. Conjusteau, and H. Mabuchi, "Finesse and sensitivity gain in cavity-enhanced absorption spectroscopy of biomolecules in solution," *Opt. Express*, vol. 14, pp. 10441-10451, 2006.

[13] P. Russell, "Photonic crystal fibers," *Science*, vol. 299, pp. 358-362, 2003.

[14] J. M. Fini, J. W. Nicholson, R. S. Windeler, E. M. Monberg, L. Meng, B. Mangan, A. DeSantolo, and F. DiMarcello, "Low-loss hollow-core fibers with improved single-modedness," *Opt. Express*, vol. 21, pp. 6233-6242, 2013.

[15] T. Ritari, J. Tuominen, H. Ludvigsen, J. Petersen, T. Sørensen, T. Hansen, and H. Simonsen, "Gas sensing using air-guiding photonic bandgap fibers," *Opt. Express*, vol. 12, pp. 4080-4087, 2004.

[16] Y. Hoo, W. Jin, H. Ho, J. Ju, and D. Wang, "Gas diffusion measurement using hollow-core photonic bandgap fiber," *Sen. Actuators B*, vol. 105, pp. 183-186, 2005.

[17] A. Cubillas, M. Silva-Lopez, J. Lazaro, O. Conde, M. N. Petrovich, and J. M. Lopez-Higuera, "Methane detection at 1670-nm band using a hollow-core photonic bandgap fiber and a multiline algorithm," *Opt. Express*, vol. 15, pp. 17570-17576, 2007.

[18] X. Li, J. Pawlat, J. Liang, and T. Ueda, "Measurement of low gas concentrations using photonic bandgap fiber cell," *IEEE Sensors J.*, vol. 10, pp. 1156-1161, 2010.

[19] F. Yang, W. Jin, Y. Cao, H. L. Ho, and Y. Wang, "Towards high sensitivity gas detection with hollow-core photonic bandgap fibers," *Opt. Express*, vol. 22, pp. 24894-24907, 2014.

[20] Y. L. Hoo, W. Jin, C. Shi, H. L. Ho, D. N. Wang, and S. C. Ruan, "Design and modeling of a photonic crystal fiber gas sensor," *Appl. Opt.*, vol. 42, pp. 3509-3515, 2003.

[21] C. Hensley, D. H. Broaddus, C. B. Schaffer, and A. L. Gaeta, "Photonic band-gap fiber gas cell fabricated using femtosecond micromachining," *Opt. Express*, vol. 15, pp. 6690-6695, 2007.

[22] A. van Brakel, C. Grivas, M. N. Petrovich, and D. J. Richardson, "Micro-channels machined in microstructured optical fibers by femtosecond laser," *Opt. Express*, vol. 15, pp. 8731-8736, 2007.

[23] Y. Hoo, S. Liu, H. L. Ho, and W. Jin, "Fast response microstructured optical fiber methane sensor with multiple side-openings," *IEEE Photonics Technol. Lett*, vol. 22, pp. 296-298, 2010.

[24] F. Yang, W. Jin, Y. Lin, C. Wang, H. L. Ho, and Y. Tan, "Hollow-core Microstructured Optical Fiber Gas Sensors," *J. of Lightwave Technol.*, 2016.

[25] R. Van Zee and J. P. Looney, *Cavity-enhanced spectroscopies* vol. 40: Academic Press, 2003.

[26] L.-S. Ma, J. Ye, P. Dubé, and J. L. Hall, "Ultrasensitive frequency-modulation spectroscopy enhanced by a high-finesse optical cavity: theory and application to overtone transitions of C_2H_2 and C_2HD," *JOSA B*, vol. 16, pp. 2255-2268, 1999.

[27] G. Gagliardi and H.-P. Loock, *Cavity-Enhanced Spectroscopy and Sensing*: Springer, 2014.

[28] X. Chen, M.-J. Li, N. Venkataraman, M. Gallagher, W. Wood, A. Crowley, J. Carberry, L. Zenteno, and K. Koch, "Highly birefringent hollow-core photonic bandgap fiber," *Opt. Express*, vol. 12, pp. 3888-3893, 2004.

[29] M. Wegmuller, M. Legré, N. Gisin, T. Hansen, C. Jakobsen, and J. Broeng, "Experimental investigation of the polarization properties of a hollow core photonic bandgap fiber for 1550 nm," *Opt. Express*, vol. 13, pp. 1457-1467, 2005.

[30] H. Chen, "Optical microwave and millimeter generation by using birefringent fiber FP cavity with pulse laser injection," *J. Infrared Milli. Waves*, vol. 28, pp. 979-986, 2007.

[31] L. S. Rothman, D. Jacquemart, A. Barbe, D. C. Benner, M. Birk, L. Brown, M. Carleer, C. Chackerian, Jr, K. Chance, L. Coudert, V. Dana, V. Devi, J. Flaud, R. Gamache, A. Goldman, J. Hartmann, K. Jucks, A. Maki, J. Mandin, S. Massie, J. Orphal, A. Perrin, C. Rinsland, M. Simth, J. Tennyson, R. Tolchenov, R. Toth, J. Auwera, P. Varanasi, and G. Wagner, "The HITRAN 2004 molecular spectroscopic database," *J. Quant. Spectrosc. Radiat. Transfer*, vol. 96, pp. 139-204, 2005.

[32] J. Parry, B. Griffiths, N. Gayraud, E. McNaghten, A. Parkes, W. MacPherson, and D. Hand, "Towards practical gas sensing with micro-structured fibres," *Meas.Sci. Technol.*, vol. 20, p. 075301, 2009.

[33] M. N. Petrovich, F. Poletti, and D. J. Richardson, "Analysis of modal interference in photonic bandgap fibres," in *2010 12th International Conference on Transparent Optical Networks*, 2010, pp. 1-4.